Effective Field Theories for Dark Matter Pairs in the Early Universe

S. Biondini,[1] N. Brambilla,[2,3] G. Qerimi,[2] and A. Vairo[2]

[1]*Department of Physics, University of Basel, Klingelbergstr. 82, CH-4056 Basel, Switzerland*

[2]*Physik-Department, Technical University Munich, James-Franck-Str. 1, 85748 Garching, Germany*

[3]*Institute for Advanced Study, Technical University Munich, Lichtenbergstrasse 2 a, 85748 Garching, Germany*

Abstract

In this conference paper, we consider effective field theories of nonrelativistic dark matter particles interacting with a light force mediator in the early expanding universe. We present a general framework, where to account in a systematic way for the relevant processes that may affect the dynamics during thermal freeze-out. In the temperature regime where near-threshold effects, most notably the formation of bound states and Sommerfeld enhancement, have a large impact on the dark matter relic density, we scrutinize possible contributions from higher excited states and radiative corrections in the annihilations and decays of dark matter pairs.

Keywords: potential NREFTs, thermal field theory, dark matter
DOI: 10.31526/LHEP.2023.375

1. INTRODUCTION

Complementary astrophysical observations strongly support the evidence that 80% of the present matter consists of dark matter (DM), and anisotropy measurements in the CMB determine precisely its relic density to be $\Omega_{\rm DM}h^2 = 0.1200 \pm 0.0012$ [1]. Despite its nature being elusive, an extensive work has been put forward and a variety of models have been constrained to reproduce this density [2, 3]. A prominent class of models involve heavy thermal DM particles, often referred to as Weakly Interacting Massive Particles (WIMPs), appearing in a typical thermal freeze-out scenario. In this proceeding, we focus on fermionic DM that experiences self-interactions through a long-range mediator within the dark sector. In particular, we consider a QED-like model and study the interactions within a thermal bath of dark photons. The proceeding is based on [4]. In Section 2, we show how to construct the DM nonrelativistic effective field theories (EFTs). In Section 3, we compute, in the EFTs, near-threshold observables. We give the DM abundance by solving the rate equations in Section 4 upon including the relevant processes. Finally, conclusions and outlook are in Section 5.

2. NREFT$_{\rm DM}$

The Lagrangian density of a dark Dirac fermion X charged under an abelian gauge group reads

$$\mathcal{L} = \bar{X}(i\not{D} - M)X - \frac{1}{4}F_{\mu\nu}F^{\mu\nu} + \mathcal{L}_{\rm portal}, \tag{1}$$

where the covariant derivative is $D_\mu = \partial_\mu + igA_\mu$, with A_μ being the dark photon field and $F_{\mu\nu} = \partial_\mu A_\nu - \partial_\nu A_\mu$. The dark fine structure constant is $\alpha \equiv g^2/(4\pi)$. Additional interactions coupling the dark photon with the SM degrees of freedom (d.o.f.), such as kinetic mixing [5, 6], are comprised in $\mathcal{L}_{\rm portal}$, which are beyond the scope of this work and thus are omitted.

We are interested in processes close to the threshold, i.e., processes involving pairs of nonrelativistic dark fermions with relative velocities $v_{\rm rel} \sim \alpha \ll 1$. The dark photons form a thermal bath of temperature T that is weakly coupled to the DM. If the latter is thermalized, then the DM momenta scale like $p \sim \sqrt{MT}$. The scales are assumed to be hierarchically ordered as

$$M \gg M\alpha \gg M\alpha^2 \gtrsim T. \tag{2}$$

In a typical freeze-out scenario, the decoupling from chemical equilibrium happens around $M/T \approx 25$. The clear separation of different scales in equation (2) allows building a tower of EFTs starting from equation (1) and extracting the relevant interactions and corresponding observables around the decoupling time. Near-threshold effects comprise the annihilation of DM pairs as well as electric transitions within the pairs. Higher multipole transitions will be suppressed at later times, i.e., smaller T. These processes play an important role in a quantitative treatment of the dynamics of the relevant d.o.f. in the early universe, and the corresponding observables appear in the evolution equations.

Integrating out hard modes leads to a nonrelativistic EFT, here dubbed NRQED$_{\rm DM}$ [7]. Hard processes such as annihilations, happening at a scale $\sim M$, are encoded at leading order in the nonrelativistic expansion in the matching coefficients of dimension-6 four-fermion operators that overlap only with S-waves.[1] At order α^3, their imaginary parts read [8, 9]

$$\mathrm{Im}\,(d_s) = \pi\alpha^2\left[1 + \frac{\alpha}{\pi}\left(\frac{\pi^2}{4} - 5\right)\right], \tag{3}$$

$$\mathrm{Im}\,(d_v) = \frac{4}{9}\left(\pi^2 - 9\right)\alpha^3. \tag{4}$$

They originate from S-wave spin-singlet ($X\bar{X} \to \gamma\gamma$) and spin-triplet ($X\bar{X} \to \gamma\gamma\gamma$) annihilations, respectively.

Next, we integrate out modes associated with the soft scale $M\alpha$. In order to enforce that the photon fields do not depend on the soft scale anymore, they are multipole expanded in the relative coordinate $\boldsymbol{r} \equiv \boldsymbol{x}_1 - \boldsymbol{x}_2$ of the pair, i.e., the distance between a fermion located at $\boldsymbol{x}_1$ and an antifermion located at $\boldsymbol{x}_2$. The effective field theory has the form of potential NRQED (pNRQED) [10, 11], and we denote it by pNRQED$_{\rm DM}$. Its La-

[1] P-wave annihilations start contributing from dimension-8 four-fermion operators and therefore are suppressed at low energies.

grangian is given by

$$\mathcal{L}_{\text{pNRQED}_{\text{DM}}} = \int d^3\boldsymbol{r}\phi^\dagger(t,\boldsymbol{r},\boldsymbol{R}) \times [i\partial_0 - H(\boldsymbol{r},\boldsymbol{p},\boldsymbol{P},\boldsymbol{S}_1,\boldsymbol{S}_2) + g\boldsymbol{r}\cdot\boldsymbol{E}(t,\boldsymbol{R})]\phi(t,\boldsymbol{r},\boldsymbol{R}) - \frac{1}{4}F_{\mu\nu}F^{\mu\nu}, \tag{5}$$

where

$$H(\boldsymbol{r},\boldsymbol{p},\boldsymbol{P},\boldsymbol{S}_1,\boldsymbol{S}_2) = 2M + \frac{\boldsymbol{p}^2}{M} + \frac{\boldsymbol{P}^2}{4M} - \frac{\boldsymbol{p}^4}{4M^3} + V(\boldsymbol{r},\boldsymbol{p},\boldsymbol{P},\boldsymbol{S}_1,\boldsymbol{S}_2) + \ldots, \tag{6}$$

$$V(\boldsymbol{r},\boldsymbol{p},\boldsymbol{P},\boldsymbol{S}_1,\boldsymbol{S}_2) = V^{(0)} + \frac{V^{(1)}}{M} + \frac{V^{(2)}}{M^2} + \ldots, \tag{7}$$

and $\boldsymbol{S}_1 = \boldsymbol{\sigma}_1/2$ and $\boldsymbol{S}_2 = \boldsymbol{\sigma}_2/2$ are the spin operators acting on the fermion and antifermion, respectively. At leading order, the static potential is the Coulomb potential $V^{(0)} = -\alpha/r$. While the photon field depends only on the center-of-mass (c.o.m.) position $\boldsymbol{R} \equiv (\boldsymbol{x}_1 + \boldsymbol{x}_2)/2$, the bilocal field of the dark pair depends on both $\boldsymbol{r}$ and $\boldsymbol{R}$ and can be decomposed into a scattering and bound state part [12]

$$\phi_{ij}(t,\boldsymbol{r},\boldsymbol{R}) = \int \frac{d^3\boldsymbol{P}}{(2\pi)^3}\left[\sum_n e^{-iE_n t + i\boldsymbol{P}\cdot\boldsymbol{R}}\Psi_n(\boldsymbol{r})S_{ij}\phi_n(\boldsymbol{P}) + \int \frac{d^3\boldsymbol{p}}{(2\pi)^3}e^{-iE_p t + i\boldsymbol{P}\cdot\boldsymbol{R}}\Psi_{\boldsymbol{p}}(\boldsymbol{r})S_{ij}\phi_p(\boldsymbol{P})\right]. \tag{8}$$

DM annihilations, inherited from the imaginary parts of the NRQED_{DM} matching coefficients, induce the following local potential

$$\delta V^{\text{ann}}(\boldsymbol{r}) = -\frac{i\delta^3(\boldsymbol{r})}{M^2}\left[2\text{Im}(d_s) - \boldsymbol{S}^2(\text{Im}(d_s) - \text{Im}(d_v))\right] + \ldots, \tag{9}$$

where $\boldsymbol{S} = \boldsymbol{S}_1 + \boldsymbol{S}_2$ is the total spin of the pair and the dots comprise annihilations with nonvanishing orbital angular momentum. The case of pNRQED at finite temperature has been studied in [13, 14], whereas an application to DM models with scalar mediators can be found in [15, 16]. The matching is done in the weakly coupled regime order by order in α, although the EFT is suited to accommodate a nonperturbative framework as well [17, 18]. The dynamics at the soft scale is encoded in the matching coefficients of $\text{pNRQED}_{\text{DM}}$ which are the potentials. The equations of motion are of the Schrödinger type, where the potentials distort the free wavefunctions into bound-state wavefunctions $\Psi_n(\boldsymbol{r})\,S_{ij}$ with discrete energies E_n or into scattering wavefunctions $\Psi_{\boldsymbol{p}}(\boldsymbol{r})\,S_{ij}$ with positive energies E_p.[2]

By exploiting EFT techniques to separate the various scales being initially intertwined in equation (1), we arrive at a thermal field theory that describes dark fermion-antifermion pairs and dark photons of energy of the order of or below the Coulomb binding energy.

[2]The spin wavefunction S_{ij} accounts for the pairs being in either a spin-singlet or spin-triplet configuration, $E_n = 2M - M\alpha^2/(4n^2) + \ldots$ and $E_p = 2M + p^2/M + \ldots = 2M + Mv_{\text{rel}}^2/4 + \ldots$.

3. NEAR-THRESHOLD PROCESSES

Though pair annihilation is a process appearing at the hard momentum scale, it encompasses near-threshold effects induced by repeated soft dark photon exchanges. Resumming such multiple rescatterings for dark fermion-antifermion pairs above the threshold, i.e., when they form a scattering state, results in a Sommerfeld-enhanced spin-averaged S-wave annihilation cross section

$$(\sigma_{\text{ann}}v_{\text{rel}})(\boldsymbol{p}) = \frac{\text{Im}(d_s) + 3\text{Im}(d_v)}{M^2}\left|\Psi_{\boldsymbol{p}}(\boldsymbol{0})\right|^2 = (\sigma_{\text{ann}}^{\text{NR}}v_{\text{rel}})\,S_{\text{ann}}(\zeta), \tag{10}$$

in the c.o.m. frame. The velocity-independent contribution from the hard scale is separated from the soft-scale-dependent Sommerfeld factor (for S-waves) [19, 20]

$$S_{\text{ann}}(\zeta) = \left|\Psi_{\boldsymbol{p}}(\boldsymbol{0})\right|^2 = \frac{2\pi\zeta}{1 - e^{-2\pi\zeta}}, \tag{11}$$

with $\zeta \equiv \alpha/v_{\text{rel}}$ and $p = Mv_{\text{rel}}/2$. On the other hand, for pairs below the threshold, the relevant observables for annihilation are the decay widths given by

$$\Gamma_{\text{ann}}^{n,\text{para}} = \frac{4\text{Im}(d_s)}{M^2}\left|\Psi_n(\boldsymbol{0})\right|^2, \tag{12}$$

$$\Gamma_{\text{ann}}^{n,\text{ortho}} = \frac{4\text{Im}(d_v)}{M^2}\left|\Psi_n(\boldsymbol{0})\right|^2, \tag{13}$$

for spin-singlet and spin-triplet S-wave bound states. We call them paradarkonium and orthodarkonium, respectively. We remark that the soft dark photon resummation effects are embedded already at the level of the Lagrangian equation (5), and that the annihilation rates follow directly from (-2) times the imaginary parts of the expectation values of equation (9).

Besides local interactions, the Lagrangian equation (5) contains an electric dipole term that allows for the formation of a bound state through low-energy photon emission of a scattering state and vice versa, i.e., the dissociation of a bound state by absorption of a dark photon from the thermal bath. We abbreviate the processes by bsf and bsd, respectively. Their thermal rates may be computed, using the optical theorem, from the self-energy diagrams in $\text{pNRQED}_{\text{DM}}$; see Figure 1.

Using the real-time formalism, we obtain for the bsf cross section

$$(\sigma_{\text{bsf}}v_{\text{rel}})(\boldsymbol{p}) = \frac{g^2}{3\pi}\sum_n\left[1 + n_{\text{B}}\left(\Delta E_n^p\right)\right][1 + n_{\text{B}}(E_n)] \times |\langle n|\boldsymbol{r}|\boldsymbol{p}\rangle|^2\left(\Delta E_n^p\right)^3, \tag{14}$$

where n_{B} is the Bose-Einstein distribution and $\Delta E_n^p = E_p - E_n = (Mv_{\text{rel}}^2/4)[1 + \alpha^2/(n^2v_{\text{rel}}^2)] + \ldots$. The dots stand for higher-order corrections in the energy spectrum. For the bsd width, we get the convolution integral

$$\Gamma_{\text{bsd}}^n = 2\int_{|\boldsymbol{k}|\geq|E_n|}\frac{d^3k}{(2\pi)^3}n_{\text{B}}(|\boldsymbol{k}|)\left[1 + n_{\text{B}}(E_p)\right]\sigma_{\text{bsd}}^n(\boldsymbol{k}), \tag{15}$$

where 2 is the dark photon polarization and σ_{bsd}^n is the photodissociation cross section averaged over the photon polarization, which reads

$$\sigma_{\text{bsd}}^n(\boldsymbol{k}) = \frac{1}{2}\frac{g^2}{3\pi}\frac{M^{3/2}}{2}|\boldsymbol{k}|\sqrt{|\boldsymbol{k}| + E_n^b} \times |\langle n|\boldsymbol{r}|\boldsymbol{p}\rangle|^2\Big|_{|\boldsymbol{p}| = \sqrt{M(|\boldsymbol{k}| + E_n^b)}}, \tag{16}$$

FIGURE 1: (Left) One-loop self-energy diagram of a scattering state (double solid line) in pNRQED$_{\rm DM}$; the imaginary part is related to the bound-state formation process $(X\bar{X})_p \to \gamma + (X\bar{X})_n$. (Right) One-loop self-energy diagram of a bound state (solid line); the imaginary part is responsible for the bound-state dissociation process $\gamma + (X\bar{X})_n \to (X\bar{X})_p$. The cross circled vertex denotes the electric dipole interaction in equation (5).

where E_n^b is the binding energy: $E_n^b = E_n - 2M$.

Further low-energy processes are the bound state-to-bound state deexcitation transitions, whose thermal widths are

$$\Gamma^n_{\text{de-ex.}} = \sum_{n'<n} \frac{g^2}{3\pi} \left(\Delta E^n_{n'}\right)^3 \left[1 + n_{\rm B}\left(\Delta E^n_{n'}\right)\right] \times \left[1 + n_{\rm B}\left(E_{n'}\right)\right] \left|\langle n'|\boldsymbol{r}|n\rangle\right|^2 , \tag{17}$$

and similarly for excitations

$$\Gamma^n_{\text{ex.}} = \sum_{n'>n} \frac{g^2}{3\pi} \left|\Delta E^n_{n'}\right|^3 n_{\rm B}\left(\left|\Delta E^n_{n'}\right|\right) \times \left[1 + n_{\rm B}\left(E_{n'}\right)\right] \left|\langle n'|\boldsymbol{r}|n\rangle\right|^2 , \tag{18}$$

with $\Delta E^{n'}_n = E_{n'} - E_n = (M\alpha^2/4)(1/n^2 - 1/n'^2) + \ldots$. We observe that each of the rates in equations (14), (15), (17), and (18) factorizes into a thermal part and an in-vacuum part involving the electric dipole matrix element squared. The thermal component can be further simplified, since the distribution functions $n_{\rm B}(E_n)$ and $n_{\rm B}(E_p)$ vanish exponentially for the temperature region set by equation (2). In that limit, our result for the bsf agrees with the outcomes in [21, 22] and for bsd with the ones in [13] for the hydrogen atom in QED at finite T and in [23] for the case of gluo-dissociation of heavy quarkonium in QCD. Eventually, the determination of the thermal rates reduces to evaluating the dipole matrix elements.

Finally, we comment on the coupling constant. Since in the fundamental theory (1) the dark photons couple only to the dark matter fermions, the coupling runs with one flavor at scales larger than M, while it is frozen at the value $\alpha = \alpha(M)$ at scales below M. Thus, the coupling constant appearing in the thermal rates discussed so far is in fact a constant.

4. RATE EQUATIONS

Having presented the relevant low-energy processes and the corresponding thermal rates, we include them in the dynamical rate equations to derive the DM thermal abundance. Here, we rely on coupled semiclassical Boltzmann equations, which under certain circumstances, namely, for Hubble rates $H(T)$ much smaller than the bound-state decays, may be written as a single effective rate equation, given by [24]

$$\left(\partial_t + 3H\right) n = -\left\langle \sigma_{\rm eff} v_{\rm rel}\right\rangle \left(n^2 - n_{\rm eq}^2\right). \tag{19}$$

The effective cross section, thermally averaged over the velocities of the incoming unbound pair, is given by[3]

$$\left\langle \sigma_{\rm eff} v_{\rm rel}\right\rangle = \left\langle \sigma_{\rm ann} v_{\rm rel}\right\rangle + \sum_n \left\langle \sigma^n_{\rm bsf} v_{\rm rel}\right\rangle \frac{\Gamma^n_{\rm ann}}{\Gamma^n_{\rm ann} + \Gamma^n_{\rm bsd}}. \tag{20}$$

Here, $\Gamma^n_{\rm ann}$ is meant to be replaced by equation (12) or equation (13) when performing the summation over S-wave bound states. Equation (20) holds in the limit when bound state-to-bound state transitions are much smaller than $\Gamma^n_{\rm ann}$ and $\Gamma^n_{\rm bsd}$ and may be neglected, which is the so-called no-transition limit. Otherwise, it has to be replaced by a more general expression presented in [25].

First, we solve the effective Boltzmann equation (19) numerically with the effective cross section in equation (20) for the DM pairs being in the ground state and with the decay width at leading order (LO) in the matching coefficient (3), i.e., just given by the paradarkonium width $\Gamma^{\rm 1S,para}_{\rm ann} = M\alpha^5/2$. This provides our reference energy density. Then, we solve the Boltzmann equation when including the 2S state in the no-transition limit, i.e., considering equation (20) up to $n = 2$S, but still with the paradarkonium decay width at LO. The ratio of the two energy densities is given in Figure 2 by the brown-dotted line. Next, we include S-wave excited states up to 10S. In Figure 2, we plot the ratio of the obtained energy density with respect to the reference one as the orange-dotted line.

Furthermore, we consider the effective cross section beyond the no-transition limit approximation, i.e., as given in [25], and solve the Boltzmann equation for the ground state including up to $n = 2$ states, but neglecting P-wave annihilation widths, and at order α^2 in the matching coefficient (3). The ratio with respect to the reference energy density is shown as the brown-dashed curve in Figure 2, where we see that 2P-to-1S transitions affect the energy density more drastically than just including nS-states in the no-transition limit.

Finally, we evaluate the impact of $\mathcal{O}(\alpha^3)$ corrections on the 1S state. We include such corrections in the ground state annihilation width and in $\langle\sigma_{\rm ann} v_{\rm rel}\rangle$. The black solid line in Figure 2 shows the ratio of the obtained energy density with respect to our reference density. The $\mathcal{O}(\alpha^3)$ corrections in the matching coefficients result in a much larger effective cross section due to the additional annihilation channel in the orthodarkonium states. It therefore decreases the DM abundance quite significantly by about 15% for DM with a mass of 1 TeV and coupling $\alpha = 0.1$.

5. CONCLUSIONS AND OUTLOOK

In this proceeding, we have summarized the findings of the recent work [4], where we use the language of NRQED and pNRQED to describe the evolution of thermalized heavy DM pairs in the early universe. Under the hierarchy of scales (2), in the EFT dubbed pNRQED$_{\rm DM}$ (5), we compute the relevant thermal rates appearing in the evolution equations. We observe that for fermionic DM pairs the additional annihilation in the spin-triplet channel, starting at order α^3 in the matching coefficients, gives large contributions to the effective cross section.

[3] We perform a thermal average in terms of the Maxwell-Boltzmann distribution of the dark fermions, $f_{\rm MB}(v_{\rm rel}) = \sqrt{2/\pi}(M/(2T))^{3/2} v^2_{\rm rel} \exp\left[-Mv^2_{\rm rel}/(4T)\right]$.

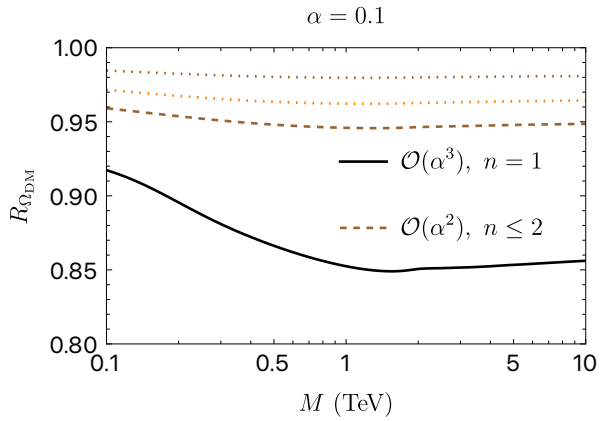

FIGURE 2: Ratios of different DM energy densities with respect to the energy density obtained from equations (19) and (20) for $n = 1$ at $\mathcal{O}(\alpha^2)$ in the matching coefficient (3), plotted as a function of the DM mass M. (Black line) The ratio for the effective cross section for $n = 1$ at $\mathcal{O}(\alpha^3)$. (Brown-dotted line) The ratio for the effective cross section for $n = 2$S at order α^2 in the matching coefficient (3), in the no-transition limit. (Orange-dotted line) The ratio for the effective cross section for $n = 10$S and matching coefficient at $\mathcal{O}(\alpha^2)$, in the no-transition limit. (Brown-dashed line) The ratio for the effective cross section for $n = 2$, but neglecting P-wave annihilation widths, at $\mathcal{O}(\alpha^2)$ in equation (9), beyond the no-transition limit approximation. We recall that the uncertainty in the measured relic density is 1%. Results are given for $\alpha = 0.1$.

Furthermore, also bound state-to-bound state transitions appear to play an important role when determining the relic density of DM. Finally, we remark that for large T the multipole expansion may break down, an issue that should be addressed in future works.

CONFLICTS OF INTEREST

The authors declare that there are no conflicts of interest regarding the publication of this paper.

ACKNOWLEDGMENTS

The work of S. Biondini is supported by the Swiss National Science Foundation under the Ambizione grant PZ00P2_185783. N. Brambilla, G. Qerimi, and A. Vairo acknowledge the support from the DFG cluster of excellence "ORIGINS" under Germany's Excellence Strategy - EXC-2094-390783311. G. Qerimi is grateful to the organizers of the NuDM-2022 conference in Egypt for the opportunity to present this research work.

References

[1] Y. Akrami et al. Planck 2018 results. I. Overview and the cosmological legacy of Planck. 2018.

[2] G. Bertone, D. Hooper, and J. Silk. Particle dark matter: Evidence, candidates and constraints. *Phys. Rept.*, 405:279–390, 2005.

[3] J. L. Feng. Dark Matter Candidates from Particle Physics and Methods of Detection. *Ann. Rev. Astron. Astrophys.*, 48:495–545, 2010.

[4] Simone Biondini, Nora Brambilla, Gramos Qerimi, and Antonio Vairo. Effective Field Theories for Dark Matter Pairs in the Early Universe: cross sections and widths.

[5] Bob Holdom. Two $U(1)$'s and Epsilon Charge Shifts. *Phys. Lett. B*, 166:196–198, 1986.

[6] Robert Foot and Xiao-Gang He. Comment on Z-prime mixing in extended gauge theories. *Phys. Lett. B*, 267:509–512, 1991.

[7] W. E. Caswell and G. P. Lepage. Effective Lagrangians for Bound State Problems in QED, QCD, and Other Field Theories. *Phys. Lett.*, 167B:437–442, 1986.

[8] Riccardo Barbieri, E. d'Emilio, G. Curci, and E. Remiddi. Strong Radiative Corrections to Annihilations of Quarkonia in QCD. *Nucl. Phys. B*, 154:535–546, 1979.

[9] Kaoru Hagiwara, C. B. Kim, and T. Yoshino. Hadronic Decay Rate of Ground State Paraquarkonia in Quantum Chromodynamics. *Nucl. Phys. B*, 177:461–476, 1981.

[10] A. Pineda and J. Soto. Potential NRQED: The positronium case. *Phys. Rev. D*, 59, 1998.

[11] Antonio Pineda and Joan Soto. The Lamb shift in dimensional regularization. *Phys. Lett.*, B420:391–396, 1998.

[12] Xiaojun Yao and Thomas Mehen. Quarkonium in-medium transport equation derived from first principles. *Phys. Rev. D*, 99(9):096028, 2019.

[13] Miguel Angel Escobedo and Joan Soto. Non-relativistic bound states at finite temperature (I): The Hydrogen atom. *Phys. Rev.*, A78:032520, 2008.

[14] Miguel Angel Escobedo and Joan Soto. Non-relativistic bound states at finite temperature (II): the muonic hydrogen. *Phys. Rev.*, A82:042506, 2010.

[15] Simone Biondini and Vladyslav Shtabovenko. Non-relativistic and potential non-relativistic effective field theories for scalar mediators. *JHEP*, 08:114, 2021.

[16] Simone Biondini and Vladyslav Shtabovenko. Bound-state formation, dissociation and decays of darkonium with potential non-relativistic Yukawa theory for scalar and pseudoscalar mediators. *JHEP*, 03:172, 2022.

[17] Nora Brambilla, Antonio Pineda, Joan Soto, and Antonio Vairo. Potential NRQCD: An Effective theory for heavy quarkonium. *Nucl. Phys.*, B566:275, 2000.

[18] Nora Brambilla, Antonio Pineda, Joan Soto, and Antonio Vairo. Effective field theories for heavy quarkonium. *Rev. Mod. Phys.*, 77:1423, 2005.

[19] A. Sommerfeld. Über die Beugung und Bremsung der Elektronen. *Ann. Phys.(1931)*, 403, 1931.

[20] S. Cassel. Sommerfeld factor for arbitrary partial wave processes. *J. Phys.*, G37:105009, 2010.

[21] Kalliopi Petraki, Marieke Postma, and Michael Wiechers. Dark-matter bound states from Feynman diagrams. *JHEP*, 06:128, 2015.

[22] Tobias Binder, Burkhard Blobel, Julia Harz, and Kyohei Mukaida. Dark Matter bound-state formation at higher order: a non-equilibrium quantum field theory approach. *JHEP*, 09:086, 2020.

[23] Nora Brambilla, Miguel Angel Escobedo, Jacopo Ghiglieri, and Antonio Vairo. Thermal width and gluo-dissociation of quarkonium in pNRQCD. *JHEP*, 12:116, 2011.

[24] John Ellis, Feng Luo, and Keith A. Olive. Gluino coannihilation revisited. *JHEP*, 09:127, 2015.

[25] Mathias Garny and Jan Heisig. Bound-state effects on dark matter coannihilation: Pushing the boundaries of conversion-driven freeze-out. *Phys. Rev. D*, 105(5):055004, 2022.